

# SDO EVE ESP Radiometric Calibration and Results

Leonid Didkovsky <sup>a</sup>, Darrell Judge<sup>a</sup>, Seth Wieman<sup>a</sup>, Tom Woods<sup>b</sup>, Phil Chamberlin<sup>b</sup>, Andrew Jones<sup>b</sup>, Frank Eparvier<sup>b</sup>, Matt Triplett<sup>b</sup>, Don Woodraska<sup>b</sup>, Don McMullin<sup>c</sup>, Mitch Furst<sup>d</sup>, and Rob Vest<sup>d</sup>

<sup>a</sup>Space Science Center, University of Southern California, 835 W. 37th St., SHS, Los Angeles, CA 90089-1341, USA;

<sup>b</sup>Laboratory for Atmospheric and Space Physics, University of Colorado at Boulder, 1234 Innovation Drive Boulder, Colorado 80303-7814, USA;

<sup>c</sup>Praxis INC, 2550 Huntington Ave. Suite 300, Alexandria, VA, 22303, USA;

<sup>d</sup>National Institute of Standards and Technology, 100 Bureau Drive, Stop 1070, Gaithersburg, MD 20899-1070, USA

## ABSTRACT

The Solar Dynamics Observatory (SDO) Extreme ultraviolet Spectro-Photometer (ESP), as a part of the Extreme ultraviolet Variability Experiment (EVE) suite of instruments, was calibrated at the National Institute of Standards and Technology (NIST) on the Synchrotron Ultraviolet Radiation Facility (SURF) Beam Line 2 in February 2007. Precise ESP alignment to the SURF beam was achieved through successive scans in X, Y, Pitch and Yaw, using a comparison of the four channels of the ESP quad photodiode as a measure of alignment. The observed alignment between the ESP and the other instruments in the EVE package was found to be in very good agreement with that measured at the Laboratory for Atmospheric and Space Physics (LASP) at the University of Colorado during EVE ESP integration. The radiometric calibration of the ESP photometers in the spectral range around 4.4 nm (central zeroth order), and the four first order channels centered at about 18.9, 25.4, 29.8, and 36.1 nm was performed with SURF synchrotron radiation. The co-alignment of the SURF beam and the ESP optical axis for each energy and injected current was determined based on quad diode (QD) photometer responses (photodiode count-rate data). This determined beam position was later used to obtain exact energy-wavelength-flux profiles for each of the calibration energies and to calculate the quantum efficiency of the ESP channels. The results of this calibration (quantum efficiencies) are compared to the previous ESP NIST calibration results at SURF Beam Line 9 and to Solar Extreme ultraviolet Monitor (SEM) efficiencies.

**Keywords:** Solar Dynamics Observatory, NIST/SURF, EVE/ESP, Radiometric calibration

## 1. INTRODUCTION

The Solar Dynamics Observatory (SDO), with its launch planned for January 2009, will provide measurements of the solar radiation and its dynamics. Dynamic changes of solar radiation in the Extreme Ultraviolet (EUV) and X-ray regions of the solar spectrum are the most efficient drivers of disturbances in the Earth's space weather environment. The Extreme ultraviolet Variability Experiment (EVE) is one of three instrument suites on SDO. EVE measures the solar EUV irradiance with unprecedented spectral resolution, temporal cadence, accuracy, and precision. Furthermore, the EVE program will incorporate physics-based models of the solar EUV irradiance to better understand how the many manifestations of solar dynamics, both short-and-long term time scales, are coupled to solar magnetic features.<sup>1-3</sup>

The Extreme ultraviolet Spectro-Photometer (ESP) is one of five EVE instruments.<sup>3</sup> The ESP design is an advanced version of the Solar and Heliospheric Observatory (SOHO) Charge, ELEMENT, and Isotope Analysis System (CELIAS) SEM instrument.<sup>4,5</sup> SEM measures EUV solar irradiance in the zeroth order (0.1 nm to 50.0 nm) and two (plus and minus) first order channels (26 nm to 34 nm) centered at the strong He II 30.4 nm

---

Further author information: (Send correspondence to L.D.)  
L.D.: E-mail: leonid@usc.edu, Telephone: 1 213 740-6343

spectral line. More than 11 years of EUV measurements have shown that SEM is a highly accurate and reliable EUV spectrometer that has suffered only minor degradation, mainly related to minimal deposition of carbon on the SEM Al filters that are near the entrance slit.

Like SEM, ESP has filters, photodiodes, and some electronics with characteristics (transmission, sensitivity, photodiode shunt resistance, etc.) that are susceptible to some change over the course of a long mission. Because of such possible degradation the instrument requires periodic calibration. The ESP calibration program includes a pre-flight calibration followed by a number of sounding rocket under-flights which carry identical copy of the flight instrument that is typically calibrated shortly before and shortly after each under-flight. Some examples and results of calibration with radiation sources for the Thermosphere, Ionosphere, Mesosphere, Energetics and Dynamics (TIMED) XUV photometer system and TIMED Solar EUV Experiment (SEE) are given by Woods et al.,<sup>6</sup> and Woodraska et. al.<sup>7</sup> SDO/EVE and EVE/ESP flight instruments have had an initial calibration at the National Institute of Standards and Technology (NIST) Synchrotron Ultraviolet Radiation Facility (SURF).<sup>8</sup> NIST SURF-III has a number of Beam Lines (BL) with different specifications and support equipment (i.e. monochromators, translation stages and calibration standards). The beamline used for a given instrument depends on the instrument's characteristics and calibration requirements, such as dimensions, spectral ranges, entrance aperture, alignment, etc. Before ESP was integrated into the EVE package, it was first calibrated on a NIST BL9. BL9 is equipped with a monochromator capable of scans through a wide EUV spectrum which allowed the instrument efficiency profile for ESP to be measured in increments of  $\delta\lambda = 0.5 \text{ nm}$  to  $1.0 \text{ nm}$  over a spectral window of about  $15 \text{ nm}$  to  $49 \text{ nm}$ . After ESP was mounted onto EVE, the second ESP calibration was performed on NIST BL2.<sup>8</sup> BL2 illuminates the instrument with the whole spectrum of synchrotron irradiance, which can be changed (shifted in the spectral range) by injecting electrons with different energies into the synchrotron ring. The intensity of the EUV beam is controlled by the current of injected electrons. Because the EUV beam consists of a wide spectrum of photon energies, this type of calibration is a radiometric calibration.

A short overview of the ESP instrument is given in Section 2. Section 3 describes an algorithm to calculate solar irradiance from the countrates measured on each of ESP's photometer channels, measurement conditions (i.e. instrument temperature, dark current, channel response, etc.), instrument calibration data and orbit parameters. Section 4 compares ESP NIST BL9 and BL2 calibrations. Calibration results are given in Section 5. Concluding remarks are given in the Summary.

## 2. A SHORT OVERVIEW OF THE SDO/EVE/ESP

ESP is a low spectral resolution (about  $4 \text{ nm}$ ) spectro-photometer with high photometric precision, high stability, and high measurement cadence. It uses mounted thin film filters, a free-standing  $5000 \text{ line/mm}$  gold bar transmission grating as the wavelength dispersive element, and photodiode detectors operating in the current mode with digitization by Voltage to Frequency Converters (VFC). All these components are flight-proven on SOHO/CELIAS/SEM,<sup>5</sup> TIMED/SEE,<sup>9,10</sup> and other space instruments.

The ESP configuration is shown in Figure 1. ESP has a filter wheel in front of the entrance aperture with three redundant Al filters, a visible light (fused silica) filter, and a dark filter. Each thin-film Al filter rejects the visible light while transmitting EUV radiation to the diffraction grating. The fused silica filter may be used to determine the amount of visible light that may reach the EUV channels as a scattered light and its signal should be subtracted from the EUV measurements. The dark filter is to measure each channel's dark (background) current.

A High-Voltage (HV) grid in front of the entrance aperture serves as a trap to low-energy electrons. High-energy Solar Energetic Particles (SEP) (more than  $40 \text{ MeV}$ ) can penetrate the ESP housing and opto-mechanical components and deposit some energy in the detectors thus adding particle related signal to the EUV signal. ESP's dark channel may be used as a proxy for the SEP related signal, which may be subtracted from the EUV channels.

The ESP has nine detector channels, including a four-channel QD at zeroth order centered at about  $4.4 \text{ nm}$ , four first order channels for wavelengths centered at about  $18.9$ ,  $25.4$ ,  $29.8$ , and  $36.1 \text{ nm}$ , and a dark channel. The QD at the zeroth order is used to track ESP solar pointing errors (or provide instrument alignment information) by analyzing the signal of horizontal and vertical diode pairs. When these four signals are summed, they also measure the solar irradiance the same way as any of four first order channels. For normal in-flight operation

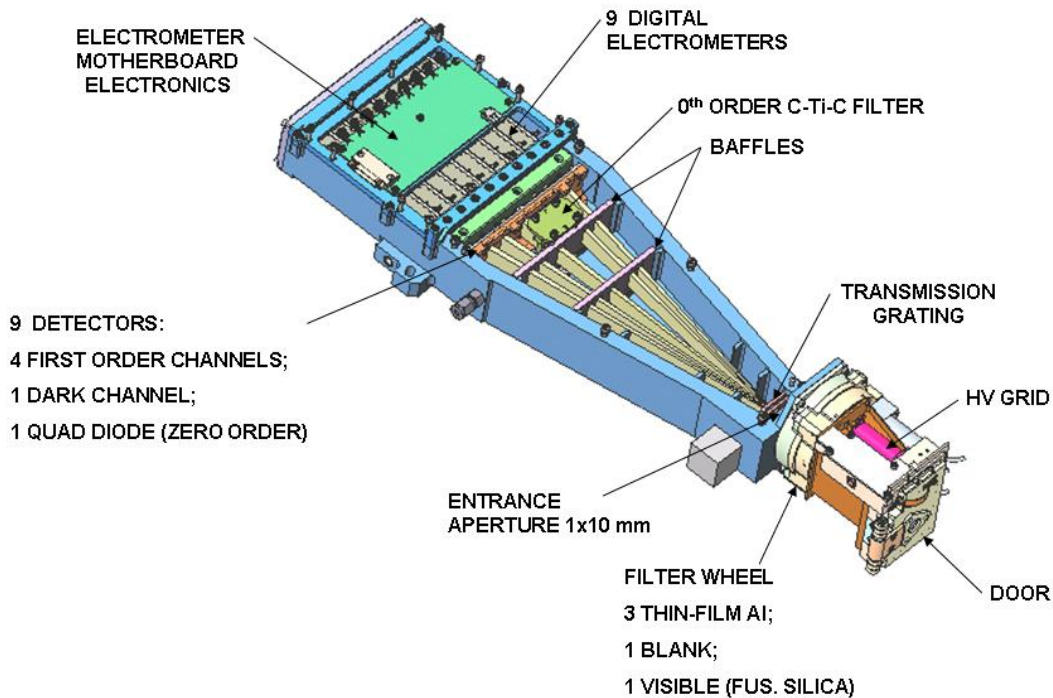


Figure 1. An overview of the ESP configuration (see details in the text).

solar irradiance detected by the zeroth order channel goes through the Al filter installed in the filter wheel and a C-Ti-C filter installed between the diffraction grating and the QD detector. These filters define the spectral window of the zeroth order channel to about 0.1 – 7.0 nm wavelength range.

The diffraction grating disperses the incident solar EUV radiation which has passed through the selected filter in the filter wheel and is detected by the four first order channels where the light generates currents in the photodiodes. The current from each diode channel is applied to the input of an electrometer (one electrometer per channel) where it is first converted to an amplified voltage signal by a low-noise high-gain operational amplifier, and then to a frequency by a Voltage-to-Frequency Converter. The output frequencies from each electrometer go to the electrometer motherboard electronics and then to the EVE Electronics Box. The ESP minimum integration time (the highest cadence) is 0.25 sec.

### 3. THE ESP SOLAR IRRADIANCE ALGORITHM

ESP measures solar irradiance in the zeroth order and four first order channels as count rates (counts per second). Each channel count rate is a function of many input parameters, e.g., intensity and spectral distribution of solar irradiance, dark currents, sensitivity to different wavelengths, distance to the Sun, degradation of the instrument, etc. All these parameters are combined in the ESP solar irradiance algorithm below. This algorithm allows us to calculate the solar irradiance based on three groups of determined parameters. The first group is based on the ESP ground tests. Parameters of this group, such as dark current characteristics, reference voltage levels, and thermal changes of these parameters, do not require any input radiation. The second group of parameters is determined based on the ESP calibration (this work) at NIST. These parameters include ESP alignment, the

efficiency of each channel, sensitivity to the changes of Field of View (FOV), characteristics of the thin-film filters, etc. The third group of parameters cannot be determined without real solar observations; they include the contribution of visible light and SEP contributions to the ESP channel signals, corrections to the EUV signal for changing dark currents, and corrections for instrument degradation based on comparisons of on orbit data with sounding rocket under-flight data.

Solar irradiance  $E_i$  (Watts/m<sup>2</sup>) for each scientific channel  $i$  is determined as

$$E_i(\lambda, t) = \frac{\frac{C_{i,eff}}{\Delta t} \frac{dG_i(T,V,TID)}{\Delta t}}{A \frac{\int_{\lambda_0-\Delta\lambda}^{\lambda_0+\Delta\lambda} R_i(\lambda, \alpha, \beta) \frac{\lambda}{hc} F_i(\lambda) d\lambda}{\int_{\lambda_0-\Delta\lambda}^{\lambda_0+\Delta\lambda} F_i(\lambda) d\lambda}} f_{degrad}(channel, t) f_{1AU}(t) - E_S \quad (1)$$

where the  $C_{i,eff}$  in the ESP irradiance algorithm (Equation 1) are the  $i$  channel effective counts per time interval  $\Delta t$ . For the time  $t_j$

$$C_{i,eff}(t_j) = C_{i,meas}(t_j) - C_{i,ch.dark}(t_j) - C_{i,particleBG}(t_j) - \Delta C_{i,vis}(t_j), \quad (2)$$

which, for each ESP channel  $i$ , are the result of subtracting the background signal (signal not related to EUV within the channels' designed bandpass) from the total measured signal ( $C_{i,meas}$ ). The background signal is composed of three parts: dark counts, measured when the dark filter is in position ( $C_{i,ch.dark}$ ), an energetic particle related signal ( $C_{i,particleBG}$ ), and visible scattered light that reaches the channel's detector ( $\Delta C_{i,vis}$ ). One of the nine ESP channels, a dark channel  $C_{dark}$ , is completely closed at all times to prevent any light from reaching it. It is possible to use the  $C_{dark}$  measurements (available at any time) as a proxy for dark counts in the science channels, and as a proxy for particle background signal. The use of the dark channel counts  $C_{dark}$  saves time during mission operations by reducing the frequency with which one needs to index the filter wheel back and forth between the dark filter and the primary observing (aluminum) filter. ESP ground tests showed a slowly varying relationship with temperature for the dark counts, namely between the dark counts,  $C_{i,ch.dark}(t_j)$ , at a given time, ( $t_j$ ), to the initial dark measurement,  $C_{i,ch.dark}(t_1)$ , at a previous time, ( $t_1$ ), when the dark filter was in place, and that the difference between the two is related to the temperature change  $\Delta T_j$

$$C_{i,ch.dark}(t_j, T_j) = C_{i,ch.dark}(t_1, T_1) - \Delta C_{i,ch.dark}(t_j, \Delta T_j), \quad (3)$$

where,

$$\Delta C_{i,ch.dark}(t_j, \Delta T_j) = C_{i,ch.dark}(t_1, T_1) - C_{i,ch.dark}(t_j, T_j) \quad (4)$$

Then, the change in a channel dark counts may be replaced with the dark channel measurements  $C_{dark}$  and the channels' dark proxy counts  $C_{i,chd.proxy}$

$$\Delta C_{i,ch.dark}(t_j, \Delta T_j) = C_{i,ch.dark}(t_1, T_1) - \frac{C_{dark}(T_j)}{C_{i,chd.proxy}(T_j)} \quad (5)$$

Thus, a channel's current dark counts at the time  $t_j$  are determined using previous measurements, *e.g.*, measurements a couple of days earlier, with the dark filter in the place at the time  $t_1$ , and the channel dark proxy, where:

$$C_{i,chd.proxy}(T_j) = \frac{C_{dark}(T_j)}{C_{i,ch.dark}(T_j)}, \quad (6)$$

where  $C_{dark}(T_j)$  and  $C_{i,ch.dark}(T_j)$  are determined for a working range of temperatures  $T$  and tabulated during ground tests. With all the above considerations, the relation for the  $C_{i,ch.dark}(t_j)$  in the Equation (2) is

$$C_{i,ch.dark}(t_j) = \frac{C_{dark}(T_j)}{C_{i,chd.proxy}(T_j)} \quad (7)$$

The degree to which each detector (channel) is shielded from energetic particles varies slightly depending on its position within the instrument (*i.e.* its location with respect to housing walls and other mechanical structures). Because of this positional dependence of shielding thickness and, accordingly, total SEP stopping

power, the channel responses to energetic particle flux were studied<sup>11</sup> for both isotropic and directional fluxes. This analysis, based on a geometrically accurate 3-dimensional model showed that the energy deposited in ESP channel detectors ( $C_{i,particleBG}$ ) by particles associated with a quiet Sun or small solar storm events, may be assumed to be within the standard deviations when determined from the dark channel signal. For solar storms associated with extreme solar flare events the particle related channel signal may be determined with position dependent modeled corrections to the signal extracted from the dark channel.

The term  $\Delta C_{i,vis}$  in Equation (2) shows the portion of the channel's signal related to scattered visible light. Laboratory measurements, in which a strong visible light source was placed in front of the ESP entrance aperture (with the filter wheel aluminum filter removed), showed very little to no visible light sensitivity in any of the ESP science channels. Nevertheless, in case of some changes in the conditions of visible light scattering, the updated  $\Delta C_{i,vis}$  may be found as

$$\Delta C_{i,vis}(t_j) = \frac{C_{fus.silica}(t_j) - C_{i,ch.dark}(t_j) - C_{i,particleBG}(t_j)}{TR_{fus.silica} + \Delta TR_{fus.silica}} f_{1AU} \quad (8)$$

where  $TR_{fus.silica}$  and  $\Delta TR_{fus.silica}$  are, respectively, the transmission of the fused silica filter and its change from pre-flight to flight conditions, ( $f_{1AU}$ ) is equal to  $1/(r)^2$ , where  $r$  is the Sun-Earth distance in Astronomical Units (AU). The amount of incoming visible light reaching the ESP entrance aperture is corrected by the relative distance to the Sun squared.

$$\Delta TR_{fus.silica} = TR_{fus.silicaflight} - TR_{fus.silicapreflight} \quad (9)$$

When the visible light signal, measured through the fused silica filter, is smaller than the sum of the channel's dark and particle background signals, then  $\Delta C_{i,vis}$  is set to zero.

Temporal changes of the channels' gain  $dG(T, V, TID)/dt$  are related to changes in the channels' temperature ( $T$ ), the reference voltage, ( $V$ ), used to calibrate the electrometer Voltage-to-Frequency Converter (VFC), and to the Total Ionizing Dose (TID), which can affect the parameters of the VFC. If the reference voltage ( $V$ ) is quite stable against TID and its temperature changes are measured during ground tests, in-flight changes of the gain after subtraction of the temperature/voltage changes give us information about the TID influence.

The ESP entrance aperture area is represented as the  $A$  variable in Equation 1.  $R(\lambda, \alpha, \beta)$  is the channel responsivity to the wavelengths in the range of the channel's spectral window, which is also a function of angular alignment, ( $\alpha$  and  $\beta$ ). The relative amplitude of the spectral radiation component  $F(\lambda)$  shown in (1) is  $F(\lambda)d\lambda / \int_{\lambda_0-\Delta\lambda}^{\lambda_0+\Delta\lambda} F_i(\lambda)d\lambda$ .  $f_{degradation}(channel, t)$  and  $f_{1AU}$  are the time and channel dependent degradation factor and a measure of the distance from the instrument to the Sun in A.U., respectively.

The term  $E_S$  is the portion of the channel's solar irradiance measurement  $E_i(\lambda, t)$  that is due to shorter wavelengths at higher diffracted orders.

$$E_S = \sum_{n=2,3} R_{S,n} E_n, \quad (10)$$

where  $R_{S,n}$  is the channel's relative sensitivity to higher orders 2 and 3,  $R_{S,n} = R_n/R_1$ .  $E_n$  is the portion of energy that reaches the channel's detector from a higher order shorter wavelength radiation.

## 4. ESP CALIBRATION AT NIST BL9 AND BL2

### 4.1 BL9 calibration results

The ESP calibration at NIST BL9 was performed to determine efficiency profiles of the ESP scientific channels as a function of wavelength. At the time of the BL9 calibration, ESP was not assembled to the EVE platform and its compact dimensions allowed it to fit into the BL9 vacuum tank for calibration. Both Al and C-Ti-C filters were removed from the instrument. The ESP was aligned to the beam using vertical and horizontal scans and tilts to find the maximal response of the zeroth order channel to the beam configuration. In the aligned position, the optical axis of ESP was coincident with the optical axis of BL9. The alignment and calibration were repeated for horizontal (dispersion direction), vertical, and 45° (between the horizontal and vertical positions). The ESP

calibration in different angular orientations around its optical axis is required because the transmission grating is sensitive to the beam polarization. Some results related to EUV measurements, polarization, and filtering with freestanding transmission gratings are given by Scime et al.,<sup>12</sup> Gruntman,<sup>13</sup> and McMullin et al.<sup>14</sup> Since the NIST SURF beam is highly polarized in the orbital plane of the orbiting electrons, we have compared the horizontal (along dispersion) and 45° efficiencies and plotted these efficiencies in Figure 2 after multiplying by the Al filter transmission. The 45° orientation was chosen as the primary orientation when the BL9 calibration results were compared to the BL2 results obtained with a unique 45° orientation of the EVE/ESP. Figure 2

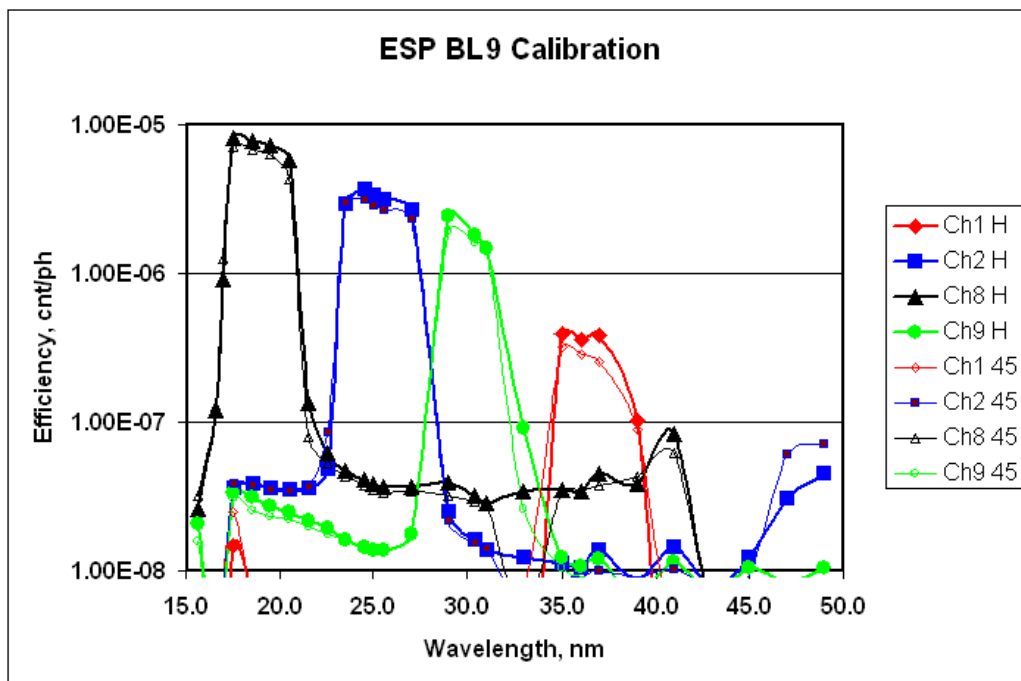


Figure 2. Efficiencies (counts/photon) for ESP first order channels are shown for the horizontal orientation (thick lines) and 45° orientation (thin lines).

shows that first order channel efficiency profiles have well determined top portions with FWHM of about 3.5 nm to 4.5 nm (a mean of 4.0 nm). The bottom portions of these profiles show some small (two orders of magnitude smaller than the peaks) deviations of the efficiencies that may add no more than approximately 2 percent to the counts related to the channel's bandwidth. These small deviations may be related to a grating non-uniformity, such as described by Balkey et al.<sup>15</sup> with a periodic change of the bar height, or to variations in of bar thickness. Some increases visible for Ch8 (around 40 nm), and Ch2 (around 50 nm) are related to the BL9 second order radiation which comes as  $\lambda/2$ , e.g. as a 24.5 nm wavelength when the BL9 is set to 49 nm wavelength.

#### 4.1.1 ESP efficiencies at the edges of the FOV

Changes in channel efficiencies related to off-pointing in the ESP pitch and yaw orientations were tested by incrementally tilting the ESP optical axis within the FOV (up to  $\pm 0.4^\circ$ ). Efficiencies are more sensitive to changes in yaw (parallel to dispersion) than to changes in pitch as the openings in the baffle structure and in the detector masks are smaller in the horizontal direction than in the vertical direction. The resulting efficiencies for the two channels with the greatest plus and minus first order dispersion angles (e.g. Ch9 = 30.3 nm; on the left edge, and Ch1 = 36.7 nm; on the right edge) are shown in Figure 3.

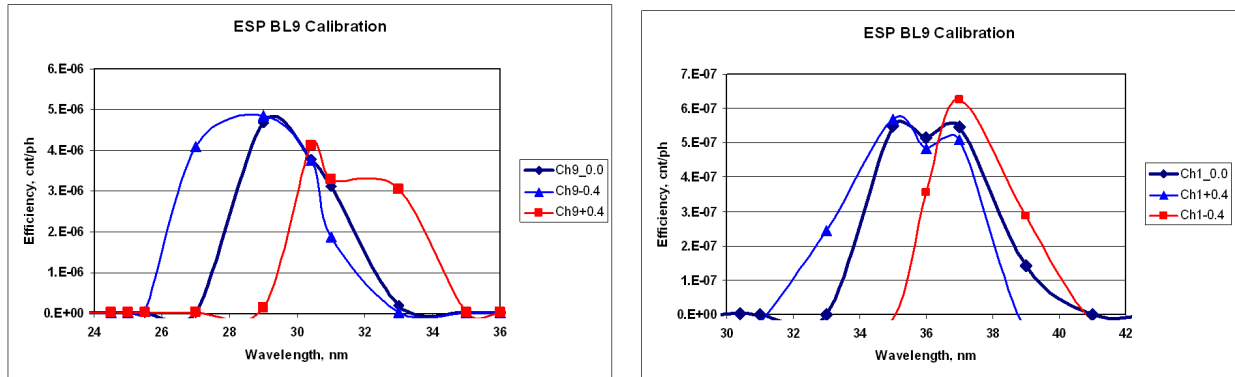


Figure 3. Left- Ch 9 efficiencies for the central ESP position (black curve) and two different yaw orientations: toward longer wavelengths (red curve), and toward shorter wavelengths (blue curve). Right- Ch1 efficiencies for the same orientations. The asymmetry of Ch1 profiles is much larger than for Ch9 profiles.

Figure 3 shows a symmetric change of the efficiency curves for Ch9 (left picture), while Ch1 tilted curves are, comparatively, quite asymmetric. As the mechanical tolerances on the detector masks (both position and opening) are less than 0.1 mm and the changes of efficiencies on the left edge of first order dispersion (Ch9) looks correct, it was assumed that openings in the baffle structures were limiting transmission to the Ch1 detector when off-pointing in yaw. These baffle openings were increased by  $\pm 0.5$  mm after the NIST BL9 calibration. This change affects (increases) the efficiencies measured (calculated) during the BL2 calibration (see the next subsection) done with the new wider openings in the baffle structure.

#### 4.1.2 Maximum ESP efficiencies determined from BL9 calibration

The maximum efficiencies measured using BL9 and the corresponding wavelengths are shown in Table 1. The values in Table 1 were obtained by multiplying the values measured at BL9 by the Al filter transmission for channels 1, 2, 8 and 9. The zeroth order quad diode channels were multiplied by the combined transmission of the Al and the C-Ti-C (zeroth order) filters, since neither of these filters were installed in ESP during the BL9 calibration.

Table 1. Maximum efficiencies (counts/photon) and corresponding wavelengths for BL9 calibration for horizontal (H), Vertical (V), Mean (H+V), and 45° positions

ESP channel	Eff. (H)	Eff. (V)	Mean (H+V) Eff.	45 deg Eff.	Wavelength, nm
Ch1	3.21E-7	4.26E-7	3.73E-7	2.62E-7	35.0
Ch2	3.69E-6	3.93E-6	3.81E-6	3.16E-6	24.5
Ch8	8.21E-6	8.31E-6	8.26E-6	7.18E-6	17.5
Ch9	2.42E-6	2.32E-6	2.37E-6	1.94E-6	29.0
QD	7.58E-7	8.37E-7	7.97E-7	6.88E-7	18.5

We have found that efficiencies for the 45° ESP position are about 23 % smaller than the mean (H+V) values and roughly proportional to the wavelength of the maximum efficiency (Table 1, right column). This difference may be explained by some instrument alignment issues, and/or the BL9 beam characteristics such as its non-uniformity and polarization. Efficiencies for the vertical orientation are about 9 % larger than those for the horizontal orientation with the exception of Ch9. This difference may also be related to the same

alignment/beam issues. Efficiency for the Quad Diode, shown as maximum, is expected to be much larger in the BL2 calibration since BL9 monochromator is limited to wavelengths longer than 15.6 nm, while shorter wavelengths than this are present in the BL2 spectrum (full un-dispersed synchrotron radiation beam).

## 4.2 BL2 calibration procedure for ESP

Before the NIST BL2 ESP calibration, the ESP baffle structure windows were enlarged in both the dispersion and non-dispersion directions by  $\pm 0.5$  mm, the ESP filter wheel with all of its filters, including the Al filters, was attached to the ESP, the C-Ti-C zeroth order filter was installed (Figure 1), and ESP was integrated into the EVE package.

The calibration of ESP took place on February 12-14, 2007 as part of the calibration for the entire EVE instrument suite. The ESP calibration procedure consisted of five steps.

The first step was an initial alignment. The alignment of the ESP to the EUV beam included determining the ESP optical axis and aligning it to the BL2 optical axis. It was done through scans in both X-and Y directions, and tilts in both U (yaw) and V (pitch) angles. The ESP alignment setup is shown in Figure 4.

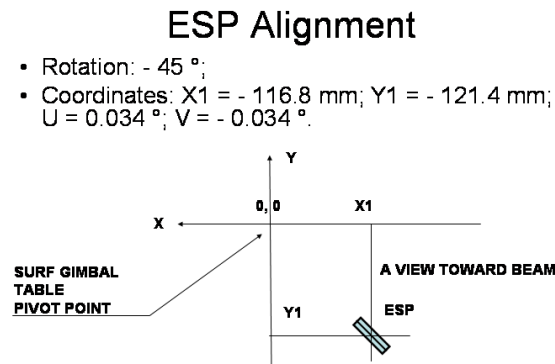


Figure 4. NIST BL2 ESP alignment setup. The coordinates  $X1=-116.8$  mm,  $Y1=-121.4$  mm,  $U=0.034^\circ$ ,  $V=-0.034^\circ$  were found to correspond to the ESP aligned position and are in a good agreement with previously determined coordinates at LASP during ESP integration tests.

The second step was to measure count rates for each channel for different radiation spectra (different beam energy and current). The third step was to determine the beam position, which might be slightly different after each injection of the electrons into the synchrotron, using X and Y scans. Typical X and Y scans are shown in Figure 5. The fourth step was an integration of the beam radiation flux over the bandpass for each channel. This step requires information about the flux profile and ESP channel responses to different wavelengths. The flux profiles for each energy used were provided by NIST, and ESP channel responses were determined from the NIST BL9 calibration (Figure 2) for the  $45^\circ$  orientation. BL9 channel responses were re-calculated from the original data by multiplying by the Al or (Al + C-Ti-C) filter transmissions and interpolated to the 0.1 nm grid used for the BL2 flux profiles. The integration of the beam radiation flux for each of the first order channels was performed throughout the spectral range of 15.6 nm to 49.0 nm used for BL9 calibration. Figure 6 shows two examples for the Ch1 and QD channels.

The second order peak, visible at around 17.5 nm for Ch1, (Figure 6; left) has an amplitude that is about 9% of that of the Ch1 peak efficiency (if the background level is subtracted), and introduces some amount of signal to the Ch1 detector, which integrates inputs from all wavelengths in the whole energy spectrum. This second order signal was subtracted from the detector's response to determine the channels' efficiency.

Good spectral selectivity of the first order channels (Figure 2) is based on the use of the diffraction grating, which limits transmission between the orders. Modeling of ESP's baffle structure<sup>16</sup> showed that it reduced stray

## ESP Typical X-and Y Scan

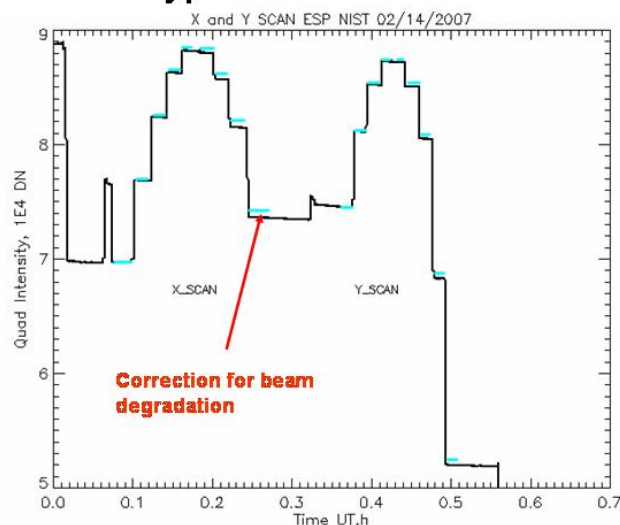


Figure 5. X and Y scans at NIST BL2 for determination of the beam center coordinates. The measured QD counts are corrected (normalized) for the beam degradation and a best fitting curve (not shown) is calculated to fit these measurement profiles.

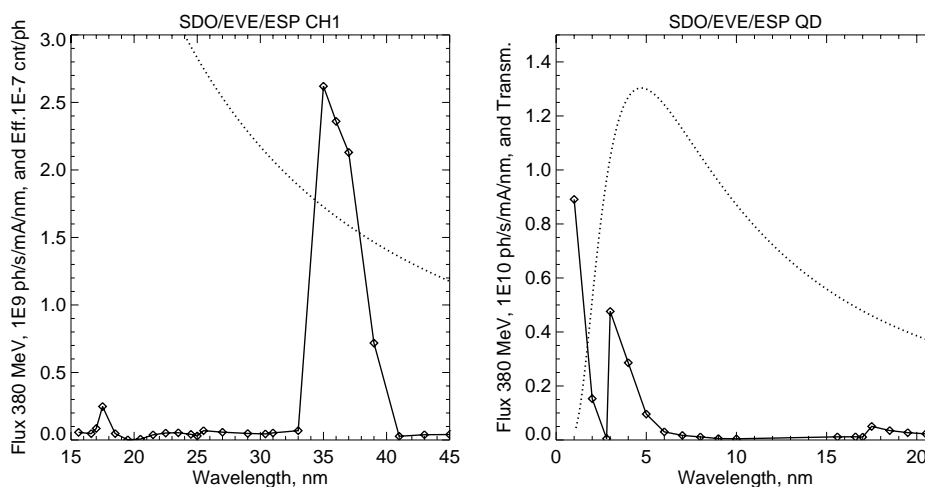


Figure 6. Left. Spectral response profile for Ch1 (diamonds) interpolated with 0.1 nm increments (solid line) and a portion of 380 MeV NIST synchrotron flux (dotted line) in the spectral window of 15.6 to 49.0 nm, which corresponds to the BL9 range of used wavelengths. A peak around 17.5 nm appears second order the Ch1 detector. Right. A transmission profile (diamonds and solid line) for combined Al and C-Ti-C filters (modeled) and a portion of 380 MeV flux (dotted line) in the spectral window of 1 – 20 nm. The 'red' (longer wavelengths) border of the zeroth order channel is limited by the low transmission of the C-Ti-C filter below 20 nm.

light by three orders of magnitude. The second order peaks, like the one visible for Ch1 (Figure 6, left) around 17.5 nm can add some counts to the detector signal and should be removed from the efficiency analysis. To determine and exclude this  $E_S$  (see Equation 1 and 10) for the second and third order contributions, several different spectra (beam energies) should be tested during the next NIST BL2 EVE/ESP calibration. A selection of spectra is required to isolate the channel's first order count-rate ( $C_{i,eff}$ ; Equation 1) from the second order signal by shifting the short wavelength edge of the beam spectrum such that it is long enough that it will not

reach the detector when diffracted in the second order.

For this calibration each channels' effective flux  $\Delta\Phi_{i,\lambda}$  was calculated in the wavelength range from  $\lambda_1 = 15.6$  nm to  $\lambda_2 = 49.0$  nm.

$$\Delta\Phi_{i,\lambda} = \sum_{\lambda_1}^{\lambda_2} \frac{\Phi_{\lambda,h} + \Phi_{\lambda,v}}{2} F_{\lambda} \Delta\lambda I_j \quad (11)$$

where  $\Phi_{\lambda,h}$  and  $\Phi_{\lambda,v}$  are horizontal and vertical fluxes modeled at NIST for each beam energy,  $F_{\lambda}$  is a relative amplitude (response) for each channels' detector (from BL9 profiles),  $\Delta\lambda$  is a 0.1 nm step, and  $I_j$  is a time dependent beam current. The flux  $\Delta\Phi_{i,\lambda}$  (Equation 11) is used in the next fifth step.

The fifth step was to determine the efficiency ( $\Psi_{i,\lambda}$ ) of each channel based on the integrated flux (Equation 11) and count rate measured by the channel (see Table 3 below, 3rd and 4th columns).

$$\Psi_{i,\lambda} = \frac{C_{i,meas}}{\Delta\Phi_{i,\lambda}}, \quad (12)$$

where  $C_{i,meas}$  are measured counts determined as a channels' count rate minus its dark current and second order signal.

Transmission of the Al filter was modeled for the determined earlier BL9 efficiencies, and the BL2 flux ( $\Delta\Phi_{i,\lambda}$ ). The filter transmission that affects the BL9 efficiency  $\Psi_{i,BL9}(\lambda)$  was a variable parameter in this model to calculate the count rates as

$$C_{i,calc}(\lambda) = \Psi_{i,BL9}(\lambda) \Delta\Phi_{BL2}(\lambda) \quad (13)$$

Filter transmission (will be measured at NIST during the next pre-flight calibration) has iteratively been changing to match the calculated (Equation 13) and measured by the ESP channels (BL2) count rates:

$$\sum_{\lambda} C_{i,calc}(\lambda) = C_{i,BL2} - C_{i,dark,BL2} - C_{i,SO,BL2}, \quad (14)$$

where  $C_{i,BL2}$  and  $C_{i,dark,BL2}$  are measured (BL2) signal and dark counts, respectively. Thus, the Equation 14 above determines the condition when the Al filter transmission (and the BL9 reference efficiency) lead to the calculated count rates that match the measured (BL2) counts for the same 45° ESP orientations. Table 3 below shows these modeled BL9 efficiencies (smaller numbers in the columns 2) and calculated BL2 efficiencies (column 3) for the first order channels. Second order influence (SO) was determined for Ch1 (Figure 6, left) and calculated to the other first order channels.

To test how the modeled (with the 380 MeV beam) Al filter transmission works for different beam energies, the BL2 flux for the 331 MeV synchrotron radiation was determined based on this modeled filter transmission, and efficiencies were calculated using measured counts as shown in the Equation (12).

## 5. ESP EFFICIENCIES FROM RADIOMETRIC CALIBRATION AT NIST BL2

Two beam energy (380 and 331 MeV) measurements were used in this work to derive the ESP efficiencies from the BL2 radiometric calibration. The details of these measurements are shown in Table 2.

The results for calculated efficiencies using radiometric calibration at BL2 for two beam energies, 380 MeV (BL2<sub>1</sub>), and 331 MeV (BL2<sub>2</sub>), as well as a comparison with the previous BL9 results are shown in Table 3. Table 3 shows that if the transmission of the Al filter (for the first order channels) corresponds to the modeled transmission, then the efficiencies determined for BL2 calibration with ESP orientation of 45° to the beam coordinates correspond to the BL9 efficiencies determined for the 45° ESP orientation (the lower efficiencies from the BL9 range at the second column of Table 3). The model of the Al filter transmission with the calculation of efficiencies for beam energy 331 MeV (4th column) shows that count rates measured at BL2 give efficiency results that are quite close (with an error of 13 % for Ch1 and 2 % to 3 % error for other channels). SOHO/SEM efficiency for Ch3 based on the February 28, 2007 NIST BL9 calibration is given as a reference in the 5th column.

In addition to the determination of the ESP efficiencies, the radiometric calibration at NIST BL2 also allowed determination of the ESP sensitivity (not shown here) to tilts within the ESPs FOV, the central wavelength for each channel, spectral ranges at the channels' half maxima, and FWHM values (Table 3).

Table 2. Counts for the beam energy of 380 MeV ( $C_1$ , and  $D_1$  for light and dark measurements) with the beam current of 0.298 mA (Feb 14, 2007 at 00:10:05 UT) and for the beam energy of 331 MeV ( $C_2$ , and  $D_2$  for light and dark measurements) with the beam current of 2.175 mA (Feb 13, 2007 at 21:51:14 UT) at NIST BL2.

Ch	$C_1$	$D_1$	$C_2$	$D_2$
Ch1	175	41	967	42.5
Ch2	2585	51	17635	50.5
Ch8	7253	42	49927	42
Ch9	1169	51	8000	51.5
QD	22048.25	50.75	saturated	50.5

Table 3. A range of maximum efficiencies (counts/photon) for different orientations at BL9 is shown in the second column. The smaller numbers for BL9 efficiencies are related to the  $45^\circ$  ESP orientation chosen to compare with efficiencies for ESP BL2  $45^\circ$  orientation. The next columns show efficiencies calculated from radiometric calibration at BL2 for beams of 380 MeV ( $\Psi_{i,\lambda}(1)$ ), and 331 MeV ( $\Psi_{i,\lambda}(2)$ ), SOHO/SEM (Ch3) efficiency as measured at BL9 Feb 28, 2007, edges of the channel's bandpass at the half maximum (HM), central wavelengths (WL), and corresponding FWHM.

Ch	BL9 Eff.	$\Psi_{i,\lambda}(1)$	$\Psi_{i,\lambda}(2)$	SEM Eff.	HM edges, nm	WL, nm	FWHM, nm
Ch1	2.62E-7 – 5.16E-7	2.62E-7	2.96E-7		34.0 – 38.1	36.05	4.1
Ch2	3.16E-6 – 3.93E-6	3.16E-6	3.10E-6		23.1 – 27.6	25.35	4.5
Ch8	7.18E-6 – 8.31E-6	7.18E-6	7.39E-6		17.2 – 20.6	18.9	3.4
Ch9	1.94E-6 – 2.42E-6	1.94E-6	1.90E-6	2.16E-7	28.0 – 31.6	29.8	3.6
QD	6.88E-7 – 8.37E-7	2.68E-5	saturated		2.9 – 5.9	4.4	3.0

## 6. SUMMARY

Precise measurement of solar EUV irradiance in five spectral windows, specifically, 4.4 nm in the central order, and 18.9, 25.35, 29.8, 36.05 nm in the first diffracted order of the transmission grating will be provided onboard SDO by the EVE/ESP instrument. An ESP solar irradiance algorithm reveals a set of ESP parameters to be measured or determined during ground-based tests, NIST calibrations, sounding rocket under-flights, and while on orbit. These parameters allow measured count rates to be properly converted to solar radiances for any short and/or long term changes of the ESP instrument. Initial estimates for some of these parameters, such as spectral responses, efficiencies, channel passbands, and central wavelengths were made during ESP calibrations at NIST Beam-Lines 9 and 2.

Calibration at BL9 was based on measurements of each channels' individual response to a set of EUV irradiances in different narrow spectral bands. The results from the BL9 calibration include each channels' spectral and angular responsivity profiles, and efficiencies. Changes of angular position of the ESP optical axis inside the FOV ( $\pm 0.4^\circ$ ) showed that openings in the baffle structure are limiting the beam on the edges of the FOV. The baffle structure has accordingly been modified to make the openings wider by  $\pm 0.5$  mm.

After integration of the ESP to the EVE platform, the calibration setup was transferred to NIST BL2, which allows calibration of larger assemblies, such as SDO/EVE. The ESP calibration was performed using spectral response profiles from the previous BL9 calibration and an EUV flux integrated over the same spectral range of 15.6 nm to 49.0 nm covered in the BL9 calibration. ESP efficiencies calculated for the BL2 calibration were compared with the efficiencies for BL9 calibration. The first order channel efficiencies determined for BL2 calibration with the  $45^\circ$  orientation of the ESP to the beam coordinates were based on the modeled Al filter transmission. These efficiencies are quite close to those determined for BL9 calibration with a difference of about 13 % for Ch1 and 2 % to 3 % for other channels.

## ACKNOWLEDGMENTS

This work has been supported in part by the SDO/EVE subcontract with the University of Colorado, award 153-5979. We thank Mike Anfinson, Richard Kohnert, Brian Templeman, Gregory Ucker, Jessica Harano of LASP for their support in the ESP NIST BL2 calibration, Matt Harmon and Hosein Ghadimi of USC for SOHO/SEM and ESP calibration at NIST BL9, Alex Farrell of NIST SURF-III for his assistance and support with ESP calibration at NIST BL2.

## REFERENCES

1. F. G. Eparvier, T. N. Woods, D. A. Crotser, G. J. Ucker, R. A. Kohnert, A. Jones, D. L. Judge, D. McMullin, and G. D. Berthiaume, "The EUV Variability Experiment (EVE) aboard the NASA Solar Dynamics Observatory (SDO)", *SPIE Proceedings*, **5660**, p. 48-55, 2004.
2. Tom Woods, Frank Eparvier, Phil Chamberlin, and Don Woodraska, "SDO EUV Variability Experiment (EVE) Space Weather Data Products", [http://lasp.colorado.edu/eve/woods\\_sdo\\_apr06\\_SpWxWeek.pdf](http://lasp.colorado.edu/eve/woods_sdo_apr06_SpWxWeek.pdf), 2006.
3. T. N. Woods, F. G. Eparvier, A. Jones, D. L. Judge, J. Lean, J. Mariska, D. McMullin, H. Warren, G. D. Berthiaume, and S. Bailey, "The EUV Variability Experiment (EVE) on the Solar Dynamics Observatory (SDO): Science plan and instrument overview", in Proc. of SOHO-17: 10 Years of SOHO and Beyond, *ESA Special Publication*, **617**, submitted, 2006.
4. D. Hovestadt, M. Hilchenbach, A. Burgi, et al. "CELIAS - Charge, Element and Isotope Analysis System for SOHO", *Solar Phys.*, **162**, p. 441-481, 1995.
5. D. L. Judge, D. R. McMullin, H. S. Ogawa, et al. "First Solar EUV Irradiances From SOHO by the CELIAS/SEM", *Solar Phys.*, **177**, p. 161-173, 1998.
6. T. Woods, E. Rodgers, S. Bailey, F. Eparvier, and G. Ucker, "TIMED Solar EUV Experiment: pre-flight calibration results for the XUV Photometer System", *SPIE Proceedings*, **3756**, p. 255, 1999.
7. D. L. Woodraska, T. N. Woods, and F. G. Eparvier, "In-Flight calibration and performance of the Solar Extreme ultraviolet Experiment (SEE) aboard the TIMED Satellite", *SPIE Proceedings*, **5660**, p. 36-47, 2004.
8. M. L. Furst, R. M. Graves, R. P. Madden, "Synchrotron ultraviolet radiation facility (SURF II) radiometric instrumentation calibration facility", *Optical Engineering*, **32 (11)**, p. 2930-2935, 1993.
9. T. N. Woods, F. G. Eparvier, S. M. Bailey, S. C. Solomon, G. J. Rottman, G. M. Lawrence, R. G. Roble, O. R. White, J. Lean, and W. K. Tobiska, "TIMED Solar EUV Experiment", *SPIE Proceedings*, **3442**, p. 180-191, 1998.
10. T. N. Woods, F. G. Eparvier, S. M. Bailey, P. C. Chamberlin, J. Lean, G. J. Rottman, S. C. Solomon, W. K. Tobiska, and D. L. Woodraska, "The Solar EUV Experiment (SEE): Mission overview and first results", *J. Geophys. Res.*, **110**, A01312, 2005.
11. L. Didkovsky, D. Judge, and S. Wieman, "Spatial and Temporal Anisotropy of SEP Fluxes at 1 AU During Solar Storms Produced by Extreme Solar Flare Events", submitted to the LWS Workshop: From the Sun towards the Earth, Boulder, 2007.
12. E. E. Scime, E. H. Anderson, D. J. McComas, and M. L. Schattenburg, "Extreme-ultraviolet polarization and filtering with gold transmission gratings", *Applied Optics*, **34**, No.4., p. 648-654, 1995.
13. M. Gruntman, "Extreme-ultraviolet radiation filtering by freestanding transmission gratings", *Applied Optics*, **34**, No.25., p. 5732-5737, 1995.
14. D. R. McMullin, D. L. Judge, C. Tarrío, R. E. Vest, and F. Hanser "Extreme-ultraviolet efficiency measurements of freestanding transmission gratings", *Applied Optics*, **43**, No.19., p. 3797-3801, 2004.
15. M. M. Balkey, E. E. Scime, M. L. Schattenburg, and J. van Beek, "Effects of gap width on vacuum-ultraviolet transmission through submicrometer-period, freestanding transmission gratings", *Applied Optics*, **37**, No.22., p. 5087-5092, 1998.
16. A. Jones, D. Alami, C. Smith, J. Craig, J. Reiter, J. Gannon, "EUV Spectrophotometer (ESP)", SDO EVE Critical Design Review Report 50004.